


Nonreciprocal photocurrent in the nonlinear response of two-dimensional modelsF. Mahmoudi and Reza Asgari ^{*}*School of Physics, Institute for Research in Fundamental Sciences (IPM), Tehran 19395-5531, Iran*

(Received 6 September 2021; revised 25 January 2022; accepted 26 January 2022; published 2 February 2022)

Monolayer two-dimensional crystalline systems with broken inversion symmetry have shown unique optical response properties. We calculate the nonreciprocal photocurrent in the nonlinear response of two-dimensional models involving the Berry connection in the presence of impurity scattering processes. Our results are based on quantum kinetic theory, where we calculate the nonequilibrium distribution function of the valence and conduction bands. We find that the significant current peak emerges at the interband absorption threshold in the electron-doped system and that the peak is remarkably sensitive to the electron density as well as the effective band masses. The current originates from trigonal warping and increases when the warping hopping parameter increases as well the band masses. A nonlinear Hall response is equally obtained for certain model Hamiltonian parameters. Our findings provide an alternative platform for nonlinear light-matter interaction engineering.

DOI: [10.1103/PhysRevB.105.085403](https://doi.org/10.1103/PhysRevB.105.085403)**I. INTRODUCTION**

The study of nonlinear electromagnetic responses [1–3] in materials can be extremely good as a classification tool and to probe material properties and has received much attention [4–10]. Nonlinear responses typically require systems that lack inversion symmetry, allowing an asymmetric photoexcitation of carriers, and to stimulate extraordinary discoveries like nonreciprocal currents [11–15] and Hall effects [16–23] in time-reversal invariant systems. The recent activities are motivated by the state-of-art experimental developments because the generation of terahertz harmonics up to the seventh order has been reported in graphene at room temperature [24–27].

It is worthwhile exploring approaches to photocurrent generation beyond conventional solar cells based on p-n junctions and magnetic elements [28,29]. A promising alternative source of photocurrent is the photovoltaic effect, a nonlinear optical response that yields net photocurrent with net polarization. The second-order optical response to a time-dependent electric field in noncentrosymmetric materials is a kinetic effect and is a type of nonlinear optical response that includes a static, DC part responsible for rectification, shift and injection currents, and the resonant photovoltaic effect [2,30–46]. Astonishingly, DC phenomena differ in those the current directions and control by an external electric field and intrinsic symmetries and materials properties. They are connected to topology and underlie photovoltaic devices [47–50].

It would be worth analyzing the photovoltaic effect in a phenomenological approach which is stemming from spatial symmetry and the possibility of expanding quantities as perturbation series [51]. Photovoltaic theory is based on asymmetry under spatial inversion in a noncentrosymmetric medium and the photocurrent is expressed by $\mathbf{J} = \langle \mathbf{E}, \kappa^l, \mathbf{E} \rangle + i\kappa^c \cdot (\mathbf{E} \times \mathbf{E}^*)$ where $\kappa^{l(c)}$ is the tensor of third

(second) rank and indicates a linearly (circularly) polarized current, and \mathbf{E} represents an applied electric field with a specific polarization. The photovoltaic currents are sensitive to light polarization and linear or circular photovoltaic effects are distinguished. The latter is because of the conversion of photon angular momentum to the translational motion of charge carriers. The symmetry argument on inversion implies that κ^l has symmetry features and, thus, the linear photovoltaic effect can occur in any piezoelectric materials. However, κ^c contains antisymmetric features and therefore it is a pseudotensor and the circularly polarized current can occur in any gyrotropic medium or chiral crystals [30].

The nonlinear optical physics has gained with the advanced two-dimensional (2D) materials, as these newly discovered materials provide a novel 2D platform to investigate a multitude of nonlinear optical effects. In addition, the nonlinear response has been studied in 2D crystalline systems represented by graphene, transition-metal dichalcogenides (TMDCs), and black phosphorus [47,49,52–55] and has exhibited a variety of fascinating phenomena owing to their unique electronic and optical properties, which differ from their bulk counterparts. The 2D materials satisfy several criteria required by an ideal nonlinear material, including a large and ultrafast nonlinear optical response, broadband and tunable optical absorption, and high chemical and mechanical stability.

The symmetry of the crystal lattices of 2D materials and their crystal orientations are vital for having the photovoltaic effect. The graphene lattice belongs to the D_{6h} point group, meaning that it is a centrosymmetric material; thus, second-harmonic generation in graphene is a forbidden nonlinear optical process, however, third-harmonic generation is allowed, which makes it a suitable material for nonlinear optical applications [25]. In contrast, TMDC monolayers belong to the D_{3h} point group at the Γ and are noncentrosymmetric, hence second-harmonic generation is the lowest-order nonlinear optical process [56,57]. For having the photovoltaic effect in TMDC at the K point, the point group might be broken.

^{*} asgari@ipm.ir

In noncentrosymmetric crystals the violation of the principle of detailed balance gives rise to an asymmetric momentum distribution for nonequilibrium electrons and holes.

It has become evident that the perfect photovoltaic calculations need a remarkable detailed knowledge of the nonthermalized charge carriers. However, general photovoltaic features can be explained by considering the band structure of the studied system. In this case, here, we consider a generic model Hamiltonian with adjustable and useful parameters to describe a gapped system with a linear or parabolic dispersion relation. To be specific, the physics of the nonlinear photocurrent of gapped graphene, phosphorene, thin-film topological insulators, and TMDC can be explained by this model using appropriate range of the parameters. We demonstrate that the static nonlinear response to polarized light, whether linear or circular polarizations, is dominated by a nonreciprocal current because of the interplay of topological properties, the Berry connection and bands topology influenced by trigonal warping and scattering processes. We refer to this response as a nonreciprocal photocurrent (NPC) where interband optical transition is considered. Our numerical results show that nonlinear optical responses are extremely sensitive to tiny changes in the materials' electronic properties.

This paper is organized as follows: The model Hamiltonian, trigonal warping, quantum kinetic theory, and photovoltaic effect in 2D systems are discussed in Sec. II. Numeric results for nonlinear DC current are presented in Sec. III, and, finally, we wrap up the main results in Sec. IV.

II. MODEL HAMILTONIAN AND QUANTUM KINETIC THEORY

We consider a direct-gap semiconductor at zero temperature with the total Hamiltonian $\mathcal{H} = \mathcal{H}_0 + \mathcal{H}_E$, where the interaction with the time-dependent external field with a monochromatic light wave is represented by $\mathcal{H}_E = e\mathbf{E}(t) \cdot \mathbf{r}$ where e is the electron charge. Let us consider a generic low-energy continuum noninteracting model Hamiltonian, which describes direct band gap semiconductors in 2D systems and can describe gapped systems with linear and parabolic dispersion relations,

$$\mathcal{H}_1 = t_0 a_0 \mathbf{k} \cdot \boldsymbol{\sigma} + \frac{\hbar^2 k^2}{2m_e} (\alpha^c + \alpha^v \sigma_z) + \frac{\Delta}{2} \sigma_z, \quad (1)$$

and trigonal warping \mathcal{H}_w contribution,

$$\mathcal{H}_w = t_1 a_0^2 (\mathbf{k} \cdot \boldsymbol{\sigma}^*) \sigma_x (\mathbf{k} \cdot \boldsymbol{\sigma}^*), \quad (2)$$

where $\mathcal{H}_0 = \mathcal{H}_1 + \mathcal{H}_w$ and the Pauli matrices $\boldsymbol{\sigma} = (\sigma_x, \sigma_y)$ acts on the two component wave functions. Notice that $\mathbf{k} = k(\cos \theta, \sin \theta)$, Δ is the band gap energy, t_0 and t_1 are hopping parameters, m_e is the electron bare mass, $(\alpha^c \pm \alpha^v)^{-1}$ is the effective conduction (valence) band mass, and a_0 is a lattice constant. To have a nonlinear photocurrent, the studied system might break the inversion symmetry, therefore, all terms in the Hamiltonian are related to broken spatial inversion symmetry. Trigonal warping causes band dispersion to be strongly anisotropic and thus the topology of the bands play an essential role in the NPC.

The dispersion relations are given by $|\mathcal{H}_0 - \varepsilon| = 0$, and thus

$$\varepsilon^s(\mathbf{k}) = h_{11} + s\sqrt{h_z^2 + |h_{12}|^2},$$

where $s = \pm$ denotes the conduction and valence bands, respectively, and

$$\begin{aligned} h_{11} &= \frac{\hbar^2 k^2}{2m_e} \alpha^c, \\ h_z &= \frac{\Delta}{2} + \frac{\hbar^2 k^2}{2m_e} \alpha^v, \\ h_{12} &= t_0 a_0 (k_x - ik_y) + t_1 a_0^2 (k_x + ik_y)^2. \end{aligned} \quad (3)$$

The effective-mass approximation restricts our theory to a small energy range in the vicinity of the band edge, although the large effective band masses ensure its applicability to high excitations. We discuss how the most physical behavior of the nonlinear optical response is sensitive to the band masses.

Nonlinear photocurrent response

The quantum kinetic theory based on the density matrix [58–60] has been successful in describing interband transitions in the presence of scattering terms.

Based on the density-matrix equation, the single-particle density matrix is given by $\rho = |\psi\rangle\langle\psi|$ and the dynamic of it obeys the quantum Liouville equation [60],

$$\frac{\partial \rho}{\partial t} + \frac{i}{\hbar} [\mathcal{H}_0, \rho] + J[\rho] = -\frac{i}{\hbar} [\mathcal{H}_E, \rho], \quad (4)$$

where $J[\rho]$ is the scattering term which takes the form within the Born approximation and we assume the correlation function $\langle U(\mathbf{r})U(\mathbf{r}') \rangle = n_i U_0^2 \delta(\mathbf{r} - \mathbf{r}')$, with n_i being the impurity density. The scattering term is given by

$$\begin{aligned} J(\langle \rho \rangle) &= \frac{1}{\hbar^2} \int_0^\infty dt' \left\langle \left[U, \left[e^{-i\mathcal{H}_0 t'/\hbar} U e^{i\mathcal{H}_0 t'/\hbar}, \rho \right] \right] \right\rangle \\ &= \frac{1}{\hbar^2} \int_0^\infty dt' \langle [U, [U(t'), \rho]] \rangle, \end{aligned} \quad (5)$$

where the average is defined over the impurity. The single-particle density matrix can be decomposed in diagonal ρ_d and off-diagonal ρ_{od} parts [60] and, thus, we can define

$$\begin{aligned} J_d[\langle \rho_d \rangle] &\sim \frac{\langle \rho_d \rangle}{\tau_1}, \\ J_{od}[\langle \rho_{od} \rangle] &\sim \frac{\langle \rho_{od} \rangle}{\tau_2}, \end{aligned} \quad (6)$$

where τ_1 and τ_2 represent the relaxation times in the intra- and interband. To get an estimate for the relaxation times τ_1 and τ_2 , we define the density matrix averaged over the impurity as $f = \langle \rho \rangle$. By making use of Eq. (5) and for the elastic scattering, the band-diagonal part of the scattering term, we

have

$$\begin{aligned} J_d[f_{d,\mathbf{k}}] &= \frac{2\pi}{\hbar} \sum_{m'\mathbf{k}'} \langle U_{\mathbf{k}\mathbf{k}'}^{mm'} U_{\mathbf{k}'\mathbf{k}}^{m'm} \rangle (f_{d,\mathbf{k}} - f_{d,\mathbf{k}'}) \delta(\varepsilon_{\mathbf{k}}^m - \varepsilon_{\mathbf{k}'}^{m'}) \\ &= \frac{2\pi}{\hbar} f_{d,\mathbf{k}} \sum_{m'\mathbf{k}'} \langle U_{\mathbf{k}\mathbf{k}'}^{mm'} U_{\mathbf{k}'\mathbf{k}}^{m'm} \rangle \left(1 - \frac{f_{d,\mathbf{k}'}}{f_{d,\mathbf{k}}}\right) \delta(\varepsilon_{\mathbf{k}}^m - \varepsilon_{\mathbf{k}'}^{m'}) \\ &= \frac{f_{d,\mathbf{k}}}{\tau_1} \end{aligned} \quad (7)$$

where the relaxation time is given by

$$\frac{1}{\tau_1} = \frac{2\pi}{\hbar} \sum_{\mathbf{k}'} \left(1 - \frac{f_{d,\mathbf{k}'}}{f_{d,\mathbf{k}}}\right) \{ \langle U_{\mathbf{k}\mathbf{k}'}^{11} U_{\mathbf{k}'\mathbf{k}}^{11} \rangle \delta(\varepsilon_{\mathbf{k}}^c - \varepsilon_{\mathbf{k}'}^c) \delta(\varepsilon_{\mathbf{k}}^c - \varepsilon_{\mathbf{k}'+\mathbf{G}}^c) \}. \quad (8)$$

Pursuing the same calculations starting by using Eq. (5) for the elastic scattering, the band-off-diagonal part, we thus have

$$\begin{aligned} \frac{1}{\tau_2} &= \frac{\pi}{\hbar} \sum_{\mathbf{k}'} \{ \langle U_{\mathbf{k}\mathbf{k}'}^{11} U_{\mathbf{k}'\mathbf{k}}^{11} \rangle \delta(\varepsilon_{\mathbf{k}'}^c - \varepsilon_{\mathbf{k}}^c) \\ &\quad - \langle U_{\mathbf{k}\mathbf{k}'}^{11} U_{\mathbf{k}'\mathbf{k}}^{22} \rangle \frac{f_{od,\mathbf{k}'}}{f_{od,\mathbf{k}}} \delta(\varepsilon_{\mathbf{k}'}^v - \varepsilon_{\mathbf{k}}^v) \\ &\quad - \langle U_{\mathbf{k}\mathbf{k}'}^{11} U_{\mathbf{k}'\mathbf{k}}^{22} \rangle \frac{f_{od,\mathbf{k}'}}{f_{od,\mathbf{k}}} \delta(\varepsilon_{\mathbf{k}}^c - \varepsilon_{\mathbf{k}'}^c) \}. \end{aligned} \quad (9)$$

Even simple models for impurity centers give the linear and circular second-order optical current. We can consider the disorder as $U(r) = U_0 \sum_i \delta(\mathbf{r} - \mathbf{r}_i)$ and define matrix elements of $U_{kk'}^{ss'}$ as

$$\begin{aligned} U_{kk'}^{ss'} &= \langle \psi_{\mathbf{k}}^s | U(r) | \psi_{\mathbf{k}'}^{s'} \rangle \\ &= U_0 \frac{h_{12}^*(k) h_{12}(k') + D_k^s D_{k'}^{s'}}{(D_k^{s^2} + |h_{12}(k)|^2)^{1/2} (D_{k'}^{s'^2} + |h_{12}(k')|^2)^{1/2}}, \end{aligned} \quad (10)$$

where the eigenvector of the system, $\mathcal{H}_0 |\psi^s\rangle = \varepsilon^s(\mathbf{k}) |\psi^s\rangle$ can be easily obtained as

$$|\psi^s\rangle = \frac{1}{\sqrt{D^{s^2} + |h_{12}|^2}} \begin{pmatrix} -h_{12} \\ D^s \end{pmatrix}, \quad (11)$$

where $D^s = h_z - s(h_z^2 + |h_{12}|^2)^{1/2}$.

The density matrix can be expanded in the powers of the electric field, $f = f^{(0)} + f^{(1)} + f^{(2)} + \dots$ [60] and thus the quantum kinetic equation provides the time evolution of

the diagonal $f_d^n = \langle \rho^n \rangle$ and off-diagonal $f_{od}^n = \langle \rho^n \rangle$ parts;

$$\begin{aligned} \frac{\partial f_d^n}{\partial t} + \frac{i}{\hbar} [\mathcal{H}_0, f_d^n] + J[f^n] &= -\frac{i}{\hbar} [\mathcal{H}_E, f_d^{(n-1)}], \\ \frac{\partial f_{od}^n}{\partial t} + \frac{i}{\hbar} [\mathcal{H}_0, f_{od}^n] + J[f^n] &= -\frac{i}{\hbar} [\mathcal{H}_E, f_{od}^{(n-1)}]. \end{aligned} \quad (12)$$

Therefore, we will get

$$\begin{aligned} \frac{\partial f_d^n}{\partial t} + \frac{i}{\hbar} [\mathcal{H}_0, f_d^n] + \frac{f_d^n}{\tau_1} &= \mathcal{D}_E(f_d^{(n-1)}) - J_d[f_d^n], \\ \frac{\partial f_{od}^n}{\partial t} + \frac{i}{\hbar} [\mathcal{H}_0, f_{od}^n] + \frac{f_{od}^n}{\tau_2} &= \mathcal{D}_E(f_{od}^{(n-1)}) - J_{od}[f_{od}^n], \end{aligned} \quad (13)$$

where $\mathcal{D}_E(f_i^{(n-1)}) = -\frac{i}{\hbar} \langle [\mathcal{H}_E, f_i^{(n-1)}] \rangle$ is the driving term and essentially contains the covariant derivative as

$$-\frac{i}{\hbar} \langle [\mathcal{H}_E, f^{(n-1)}] \rangle = \frac{e\mathbf{E}}{\hbar} \cdot \{ \nabla_{\mathbf{k}} f^{(n-1)} - i \langle [\mathcal{R}_{\mathbf{k}}, f^{(n-1)}] \rangle \},$$

where the first term on the right-hand side contains the Fermi-surface information and the second term shows the Fermi sea response and the Berry curvature effects. $\mathcal{R}_{kk'}^{ss'} = i \langle \psi_{\mathbf{k}}^s | \nabla_{\mathbf{k}'} | \psi_{\mathbf{k}'}^{s'} \rangle$ is the Berry connection and, in order to calculate it, we need to calculate $\nabla_{\mathbf{k}} |\psi^s\rangle$. Therefore, by making use of all derivatives, the Berry connection can be obtained as

$$\begin{aligned} \mathcal{R}_{kk'}^{ss'} &= i \langle \psi_{\mathbf{k}}^s | \nabla_{\mathbf{k}'} | \psi_{\mathbf{k}'}^{s'} \rangle \\ &= -i \frac{\mathbf{f}^{s'}(\mathbf{k}')}{(D^{s^2} + |h_{12}|^2)^{1/2} (D^{s'^2} + |h_{12}|^2)^{3/2}} [h_{12}^* h_{12} + D^s D^{s'}] \\ &\quad + i \frac{[(h_{12}^* \partial_k h_{12} + D^s \partial_k D^{s'}) \hat{k} + \frac{1}{k} (h_{12}^* \partial_\theta h_{12} + D^s \partial_\theta D^{s'}) \hat{\theta}]}{(D^{s^2} + |h_{12}|^2)^{1/2} (D^{s'^2} + |h_{12}|^2)^{1/2}}, \end{aligned} \quad (14)$$

where $\mathbf{f}^s(\mathbf{k}) = \nabla_{\mathbf{k}} (D^{s^2} + |h_{12}|^2)/2$ and $\mathcal{R}_{\mathbf{k}}^{s's} = \mathcal{R}_{\mathbf{k}}^{*ss'}$ is satisfied. Notice that the crystal asymmetry has been usually incorporated into the Berry connection.

It will be clear soon that the off-diagonal contributions are related to NPC on nonlinear optical response. Notice that $f_d^{(0)} = f_0(\varepsilon_k)$ and $f_{od}^{(0)} = 0$ where $f_0(\varepsilon(k))$ is the equilibrium Fermi-Dirac distribution function. In this stage we follow the perturbation recipe to calculate the first- and second-order density matrices, $f_{od,\mathbf{k}}^{(1)}(t)$, $f_{d,\mathbf{k}}^{(1)}(t)$ and $f_{od,\mathbf{k}}^{(2)}(t)$ and $f_{d,\mathbf{k}}^{(2)}(t)$.

Therefore, all single-density-matrix terms can be written as

$$\begin{aligned} f_{d,\mathbf{k}}^{(1)}(t) &= \int_{-\infty}^t dt' e^{-\frac{t-t'}{\tau_1}} \{ e\mathbf{E}(t') \cdot \nabla_{\mathbf{k}} f_0(\varepsilon) - J_d[f_{od,\mathbf{k}}^{(1)}(t')] \}, \\ f_{od,\mathbf{k}}^{(1)}(t) &= \int_{-\infty}^t dt' e^{-\frac{t-t'}{\tau_2}} e^{-ie^c(t-t')/\hbar} \{ -e\mathbf{E}(t') \cdot i\mathcal{R}_{\mathbf{k}}^{12} [f_0(\varepsilon^c) - f_0(\varepsilon^v)] - J_{od}[f_{d,\mathbf{k}}^{(1)}(t')] \} e^{ie^v(t-t')/\hbar}, \\ f_{d,\mathbf{k}}^{(2)}(t) &= \int_{-\infty}^t dt' e^{-\frac{t-t'}{\tau_1}} [e\mathbf{E}(t') \cdot \{ \nabla_{\mathbf{k}} f_{d,\mathbf{k}}^{(1)}(t') \} - J_d[f_{od,\mathbf{k}}^{(2)}(t')]], \\ f_{od,\mathbf{k}}^{(2)}(t) &= \int_{-\infty}^t dt' e^{-\frac{t-t'}{\tau_2}} e^{-ie^c(t-t')/\hbar} \\ &\quad \times [e\mathbf{E}(t') \cdot \{ \nabla_{\mathbf{k}} f_{od,\mathbf{k}}^{(1)}(t') - i f_{od,\mathbf{k}}^{(1)}(t') [\mathcal{R}_{\mathbf{k}}^{11} - \mathcal{R}_{\mathbf{k}}^{22}] \} - J_{od}[f_{d,\mathbf{k}}^{(2)}(t')]] e^{ie^v(t-t')/\hbar}. \end{aligned} \quad (15)$$

Now, by considering whether the external electric field is that of linearly or circularly polarized light, namely $\mathbf{E}(t) = E(\hat{i} \cos \theta_p \cos \omega t + \hat{j} \sin \theta_p \sin \omega t)$ where $\theta_p = 0$ or $\pm\pi/4$, respectively, we can solve Eq. (15) and then the optical current will be obtained by

$$\mathbf{j} = -\frac{e}{\hbar} \int \frac{d\mathbf{k}}{4\pi^2} \text{Tr}[\mathbf{v}\mathbf{f}_{\mathbf{k}}], \quad (16)$$

where the velocity tensor $\hbar\mathbf{v} = \frac{D\mathcal{H}_0}{D\mathbf{k}}$. By expanding the covariant derivative, the velocity is given by $\hbar\mathbf{v} = \nabla_{\mathbf{k}}\varepsilon(k) - i[\mathcal{R}, \mathcal{H}_0]$ and, eventually, the total current is

$$\begin{aligned} \mathbf{j}^s &= \mathbf{j}_d^s + \mathbf{j}_{od}^s \\ &= -\frac{e}{\hbar} \int \frac{d\mathbf{k}}{4\pi^2} \{ \nabla_{\mathbf{k}}\varepsilon^s(k) f_{\mathbf{k}} \delta_{ss'} - i\mathcal{R}_{\mathbf{k}}^{s's} [\varepsilon^s(k) - \varepsilon^{s'}(k)] f_{\mathbf{k},ss'} \}, \end{aligned} \quad (17)$$

where the first and second terms refer to the intra and interband contributions, respectively. To capture the TNPV current, the electric field needs to be incorporated into the time-evolution operator, leading to the scattering term.

III. NUMERICAL RESULTS AND DISCUSSIONS

In this section, we present our results of the second-order optical current provided by Eqs. (15) and (17). We set $\Delta = 0.32$ and $t_0 = 2.34$ eV, $a_0 = 1.82\sqrt{3}\text{\AA}$. We also set $\alpha^c = 0.5$ and $\alpha^v = 0.75$, otherwise, we explicitly give those values. We consider distinct values of the trigonal warping term t_1 , about -0.34 , -0.64 , and -0.94 eV and the relaxation time is considered to be a constant; $\tau = \tau_1 = \tau_2$, varying (0.5–1.5) ps. The electron densities are considered to be $(1-4) \times 10^{12} \text{ cm}^{-2}$. Moreover, we ignore J_d and J_{od} terms appeared in Eq. (15) in our numerical calculations.

Notice that the Hamiltonian parameters can be fixed for a real system, for instance, $\Delta = 1.82(0.91)$, $t_0 = 2.34$ (0.48 along the x direction only), $t_1 = -0.34(0.003)$ eV, $a_0 = 1.82\sqrt{3}$ (along x is 2.23 and y is 1.64) \AA and $\alpha^c = 0.02(1.660)$ and $\alpha^v = 3.08(0.683)$ for MoS₂ (phosphorene), respectively [61,62]. The averaged band masses, $\sqrt{m_x m_y}$, are considered for phosphorene.

To begin with, the contour plot of the dispersion relations of the Hamiltonian associated with the conduction and valence bands is shown in Fig. 1 for the two different warping values $t_1 = -0.34$ and -0.94 eV. The anisotropic behavior of the dispersion relations increase upon increasing not only the deeper energy but also the value of warping. The difference between the band masses can manage a discrepancy between the conduction band and the valence band.

The nonlinear DC currents caused by Eq. (15) arising from two time-dependent electric fields; the one originated from $f^{(2)}$ by itself and another came from $\nabla_{\mathbf{k}} f^{(1)}$. Since the electric field is represented as $\mathbf{E} \cos(\omega t)$, the nonlinear current is proportional to $\cos^2(\omega t) = \frac{1}{2} + \frac{1}{2} \cos(2\omega t)$ where the constant term provides the nonlinear DC current.

The nonlinear DC currents are presented in Fig. 2 in terms of warping values along the x and y directions. The value of the nonlinear DC current increasing by increasing the trigonal warping term t_1 and its jump emerges at the interband absorption threshold. By increasing the light frequency, electrons

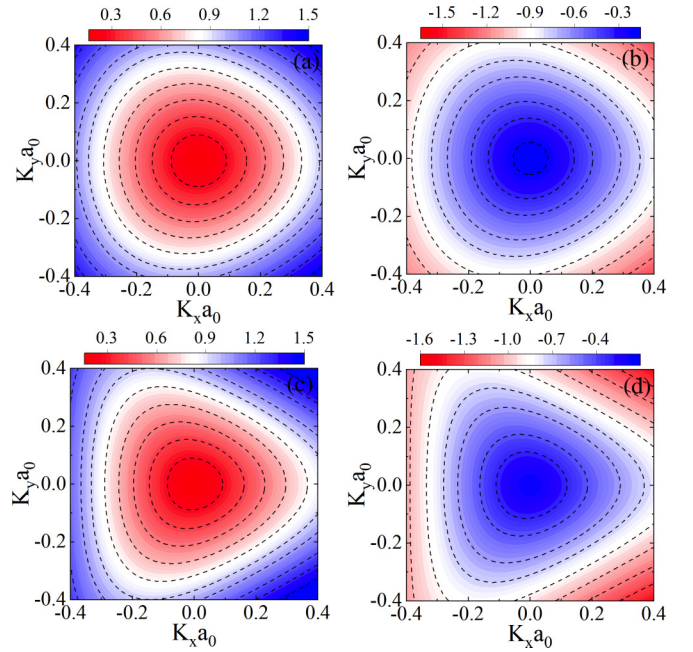


FIG. 1. Contour plot of the energy dispersion of the conduction and valence bands around with iso-energy dashed lines as a guide to the eye for different $t_1 = -0.34$ and -0.94 eV in the top and bottom panels, respectively. The valence bands are plotted in panels (b) and (d); however, the conduction bands are shown in panels (a) and (c). Strong trigonal warping in the bands causes a more discrepancy between the valence- and conduction-band dispersions with different band masses.

deeper in the valence band are excited to the conduction band; increasing the NPC. The existence of the increasing current occurs until the optical interband transition rate is nonzero and the latter depends strongly on the structure of the band structure or the band gap and the value of the effective band masses. For instance, the range of the increasing of the current as a function of the light frequency increases when the conduction-band mass grows with respect to the valence-band mass. Interestingly, by applying the electric field along the x direction, $J_y^{(2)}$ is nonzero for the given values of α^c and α^v and a nonlinear Hall response appears. The optical nonlinear Hall response becomes more minimal by reducing the effective band masses in the conduction and valence bands. Nonlinear optical responses are extremely sensitive to small changes in the material's electronic properties.

The second-order density matrix has several terms and a dominate term contains $\mathcal{R}_{\mathbf{k}}^{12}[\nabla_{\mathbf{k}}\varepsilon^c(k) - \nabla_{\mathbf{k}}\varepsilon^v(k)][f_0(\varepsilon^c(k)) - f_0(\varepsilon^v(k))]/[-\hbar\omega + \varepsilon^c(k) - \varepsilon^v(k) + i\hbar\tau^{-1}]^2$. Our results show that the injection contribution, which comes from the fact that the electron and holes have different velocities, and that the coherent \mathbf{k} and $-\mathbf{k}$ excitations are imbalanced, as well as the higher-order pole current, are contributions to obtain the DC nonlinear optical response in the studied system [30]. Both depend on the scattering time values, and thus the current is enhanced if the relaxation time increases. However, anomalous current and double resonant current include a negligible contribution to the nonequilibrium DC optical response. On the other hand,

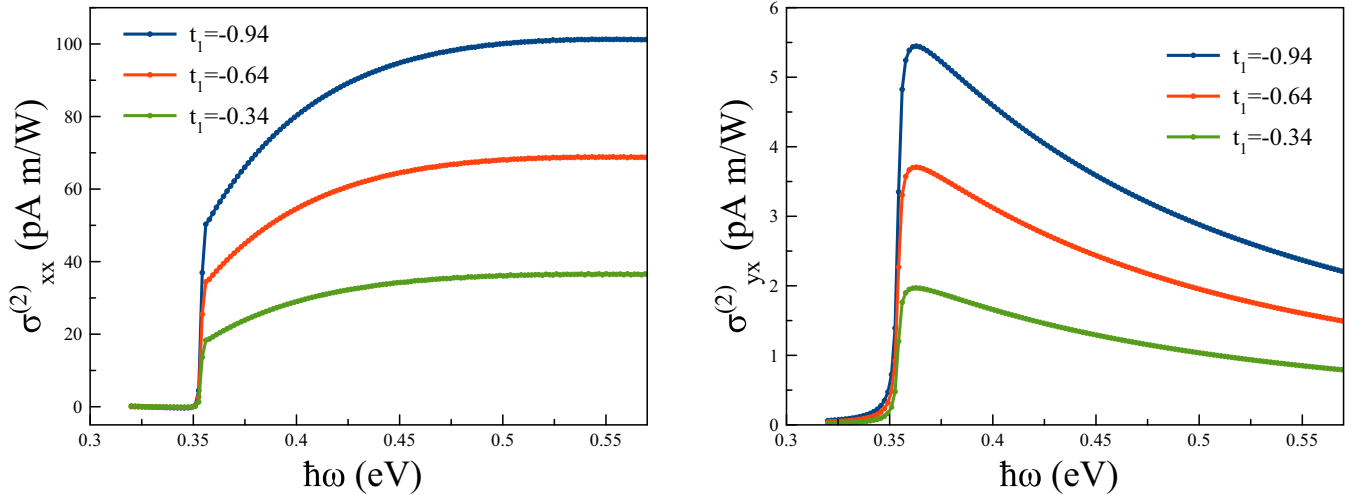


FIG. 2. Second-order optical response, $\sigma_{ij}^{(2)} = J_i^{(2)}/|E_j|^2$ (in units of pA m/W) as a function of $\hbar\omega$ (in units of eV) for linearly polarized light, $\theta_p = 0$ along the x and y directions for different hopping terms t_1 in eV. The nonlinear Hall response is nonzero for the chosen parameters. The relaxation time $\tau = 0.5$ ps and the electron density is $n = 1 \times 10^{12} \text{ cm}^{-2}$. The NPC jump appears at unique energies because of the $(\Delta + 2\varepsilon_F)$ values. The existence of the increasing current occurs until the optical interband transition rate is nonzero and the latter depends strongly on the structure of the band structure or the band gap and the value of the effective band masses. Strong trigonal warping in the valence band causes a large discrepancy between the valence- and conduction-band dispersions with different band masses.

the resonance photovoltaic effect is also negligible owing to particle-hole asymmetry.

It is worth mentioning that the shift current mechanism originates from the difference of the wave function center of the electron and hole band states. The shift current ignores the kinetic processes of relaxation of photoexcited electrons. Moreover, the shift current is an intrinsic contribution and does not depend on impurity or the relaxation-time process. For an almost nonpolar system such as MoS₂, phosphorene, and gapped graphene, the shift current tends to be remarkably small. Accordingly, it is necessary to treat the nonlinear optical current as a kinetic phenomenon that is missing in the shift current [63].

To examine the impact of the band masses, we present the nonlinear response in Fig. 3 along the x and y directions for various α^v for linearly polarized light with $n = 10^{12} \text{ cm}^{-2}$. The $\sigma_{ij}^{(2)}$ becomes smaller by reducing the band masses along both directions. However, our numerical results show that the nonlinear response rises upon increasing the band masses, too. The position of the jump changes due to the variations in the Fermi energy. These results indicate that the NPC is significantly sensitive to the band masses.

Now we devote our attention to the polarization dependence of the nonlinear DC current. As we mentioned earlier, the linear response is allowed for noncentrosymmetric materials and the circular response is determined in gyrotropic materials. The linear and circular polarization dependence of the NPC are shown in Fig. 4. The linear polarization current is smaller than the circular polarization current. Since the linear polarization is a sum of the right- and left-circular polarizations, apparently, there are cancellation terms in the linear polarization current. This suggests a strong unidirectional current in response to circularly polarized light. The nonlinear Hall response $J_y^{(2)}$ becomes smaller in the circularly polarized light. The negative value of the nonlinear Hall response originates from the intraband contribution.

Interestingly, the current does change with the Fermi energy besides the optical transition point owing to $\Delta + 2\varepsilon_F$. Notice that the many-body electron-electron interaction-induced renormalization of the self-energy and a large and nonlinear band-gap renormalization upon adding free carriers to the conduction band occurs. Therefore, the position of the peak jump is renormalized by quantum many-body effects and we ignore those effects. The $\sigma_{xx}^{(2)} = J_x^{(2)}/|E_x|^2$ shows general features as Fig. 2. In addition, by increasing the electron density, the Sommerfeld factor [64,65] shows up and our theory

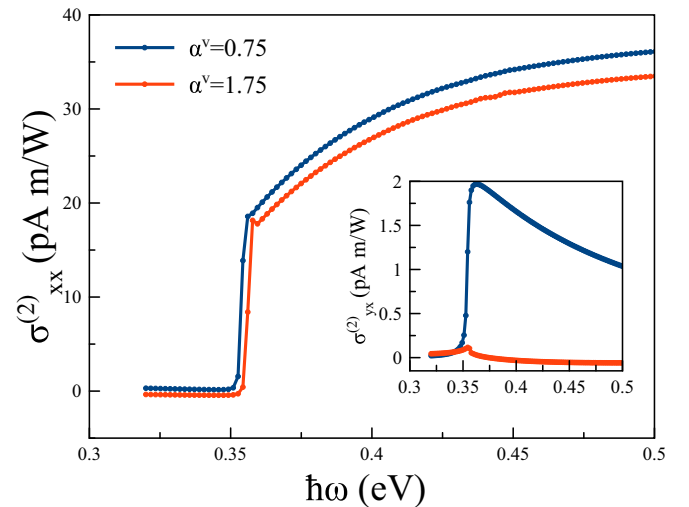


FIG. 3. Second-order optical response, $\sigma_{xx}^{(2)} = J_x^{(2)}/|E_x|^2$ (in units of pA m/W) as a function of $\hbar\omega$ (in units of eV) for linearly polarized light, $\theta_p = 0$ along the x direction for different masses, α^v for giving $\alpha^c = 0.5$. Inset shows the nonlinear response along the y direction. The $\sigma_{ij}^{(2)}$ response becomes smaller by increasing α^v . The relaxation time $\tau = 0.5$ ps and the electron density is $n = 1 \times 10^{12} \text{ cm}^{-2}$.

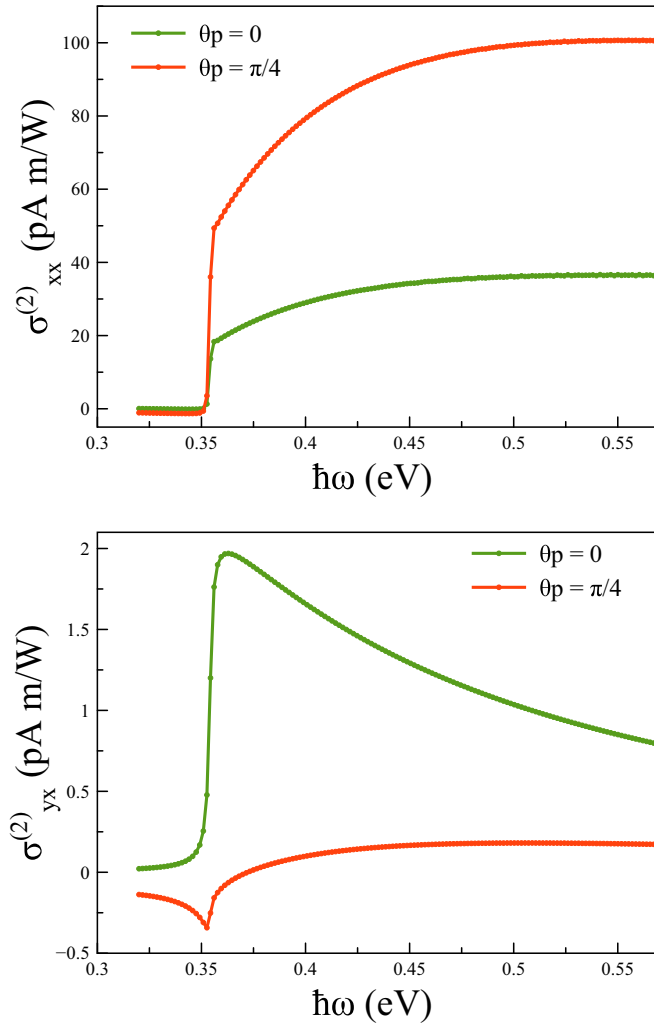


FIG. 4. Second-order optical response, $\sigma_{ij}^{(2)} = J_i^{(2)}/|I_{E_j}|^2$ (in units of pA m/W) as a function of $\hbar\omega$ (in units of eV) for different polarizations, $\theta_p = 0$ and $\frac{\pi}{4}$ along the x and y directions. The relaxation time $\tau = 0.5$ ps, the warping $t_1 = -0.34$ eV, and the electron density $n = 1 \times 10^{12}$ cm $^{-2}$. The nonlinear Hall response $J_y^{(2)}$ becomes smaller in circularly polarized light.

also accounts for the Sommerfeld factor. To emphasize this process, Fig. 5 shows the nonlinear DC current found using the different electron densities. Our numerical results show that the peak also increases with growing α^v or decreasing α^c . Therefore, the peak disappears by making use of larger α^c and smaller α^v values. Our numerical results show that there is also a tiny bump around the peak for the $\sigma_{yx}^{(2)} = J_y^{(2)}/|I_{E_x}|^2$ in a greater electron density.

To explore the peak around the interband transition, we focus on the Sommerfeld factor [64] (for instance see Fig. 5). The spectral function and the optical linear susceptibility are given by the real-space Green's function. In addition, $f_{od}^{(1)}(\mathbf{k})$ can be obtained from the \mathbf{k} -space Green's function. The Sommerfeld factor implies a peak around the optical transition in the density of states, hence we expect a peak in the current near the optical transition, which indicates the large density of states. The latter is proportional to $1/a_b^{*2}$ where the effective Bohr radius $a_b^* = \hbar^2 \epsilon / m^* e^2$ with the reduced effective mass

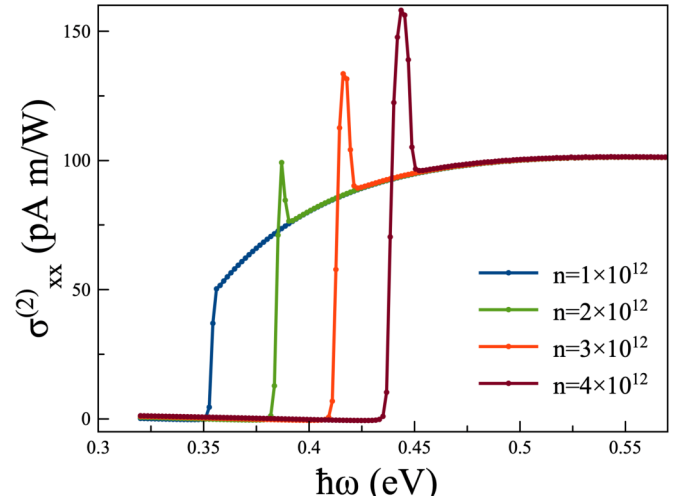


FIG. 5. Second-order optical response, $\sigma_{xx}^{(2)} = J_x^{(2)}/|I_{E_x}|^2$ (in units of pA m/W) as a function of $\hbar\omega$ (in units of eV) for linearly polarized light, $\theta_p = 0$ along the x direction and different electron density in units of cm $^{-2}$. The relaxation time $\tau = 0.5$ ps and the warping term is $t_1 = -0.94$ eV. The magnitude of the peak is sensitive to the electron density owing to the Sommerfeld factor. This peak disappears by increasing the values of α^c and α^v .

between the valence and conduction bands; $m^* = m_e(\alpha^{v2} - \alpha^{c2})/2\alpha^c$. This result is in good agreement with our numerical results explained earlier. The peak in optical absorption near the band edge originates from the Sommerfeld factor [65] and its amplitude depends on material parameters.

We explore the effect of the relaxation time τ on the NPC and results are shown in Fig. 6. The current changes significantly by changing the relaxation time and when τ is large, the NPC can be larger, which is helpful for photovoltaic solar cell applications. Terms of the form $(f_0^c - f_0^v)$

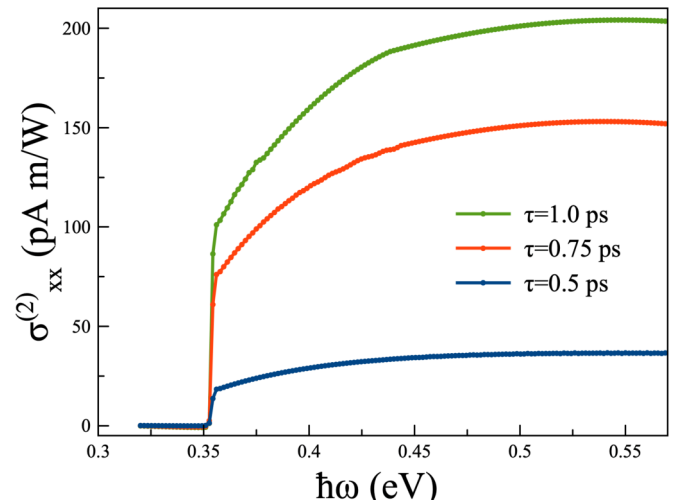


FIG. 6. Second-order optical response, $\sigma_{xx}^{(2)} = J_x^{(2)}/|I_{E_x}|^2$ (in units of pA m/W) as a function of $\hbar\omega$ (in units of eV) for linearly polarized light, $\theta_p = 0$ along the x direction and different τ in ps. The warping term is $t_1 = -0.34$ eV and the electron density is $n = 1 \times 10^{12}$ cm $^{-2}$.

are always present in $f_{od}^{(2)}$ [47,60], where $f_0^{c(v)}$ is the Fermi-Dirac distribution function in the conduction (valence) bands. However, the denominator contains expressions of the form $[-\hbar\omega + (\varepsilon^c - \varepsilon^v) + i\hbar/\tau]^2$, which tend to a smaller value as τ increases, and thus the peak becomes stronger although its width does not change because of the $(f_0^c - f_0^v)$ term. Therefore, integrating over k , a larger current emerges owing to the stronger peak. The presence of τ can also be viewed as a reflection of Kramers symmetry breaking by the warping term, which causes the excited carrier distribution to be asymmetric on the two sides of the conduction band. Although the $\sigma_{yx}^{(2)}$ behaves nonlinearly in terms of τ , our numerical results show that the nonlinear Hall response $\sigma_{yx}^{(2)}$ behaves linearly.

In the system explored here the recombination rate is smaller than the excitation rate because (i) in noncentrosymmetric crystals the principle of detailed balancing is broken for nonequilibrium photoexcited carriers [36], (ii) the electron mobility is greater than the hole mobility implying different band masses, and (iii) a separation between the center of the electron wave-packet and hole packet in real space occurs, which becomes larger when the discrepancy between two bands increase.

IV. CONCLUSION

Nonlinear response can be extremely good as a classification tool to study materials and allows us to detect novel physics that are invisible in linear optical response. We have investigated the second-order static steady-state photocurrent in a generic two-dimensional crystal and shown nonlinear DC currents along x and y directions. A strong unidirectional current in response to circularly polarized light is identified. The current increases with the charge relaxation time and trigonal warping coefficient. Our theory incorporates interband scattering, including electric-field-induced scattering effects. The topological nonreciprocal photocurrent results from topological effects through the Berry connections, band-mass discrepancy between the electron and hole, which leads to a change in the electron wave packet regarding the hole wave packet, and trigonal warping in the bands which makes the wave packet different between the conduction and valence bands. We have shown that the magnitude of the nonlinear DC current depends on material parameters as well as the relaxation time. Furthermore, a finite nonlinear Hall response appears for certain values of the effective band masses. Our findings provide an alternative platform for nonlinear light-matter interaction engineering and will stimulate state-of-art experiments.

The nonequilibrium distribution to second order in the electric field has a nonzero time average, resulting in a DC nonlinear optical response. The time average of the total acceleration in the system is nonzero, since the acceleration oscillates in time as well as the distribution of excited carriers. This nonzero time average represents a constant acceleration. The angular average of the acceleration is nonzero owing to the anisotropy of the excitation originated from trigonal warping. Subsequently, excited carriers possess a constant acceleration, and this needs to be controlled by scattering process, represented by the relaxation time. The presence of τ

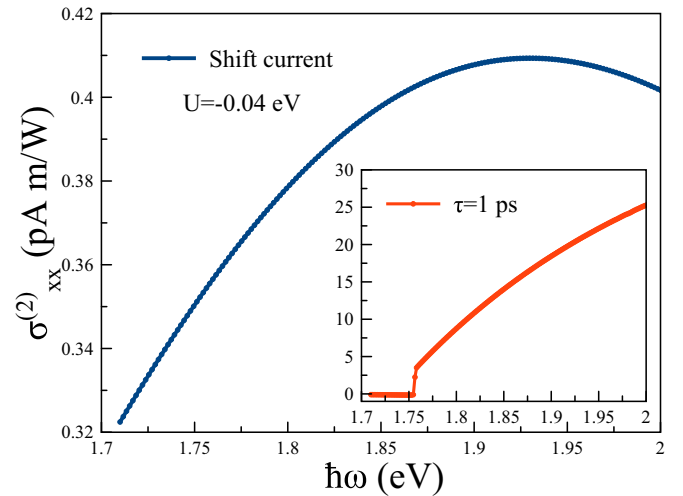


FIG. 7. Second-order optical response $\sigma_{xx}^{(2)} = J_x^{(2)}/|E_x|^2$ (in units of pA m/W) as a function of $\hbar\omega$ (in units of eV) along the x direction for circularly polarized light $\theta_p = \pi/4$ in MoS₂ with broken mirror symmetry $U = -0.04$ eV by using Eq. (A3) for $n = 5 \times 10^{12}$ cm⁻². Inset shows the same quantity using the density matrix for $\tau = 1$ ps. The shift current represents an intrinsic property and does not depend on impurities. It ignores the kinetic processes of relaxation of photoexcited electrons. Moreover, the shift current shows a remarkably small nonlinear optical response for a nonpolar system.

can also be viewed as a reflection of Kramers symmetry breaking by the warping contribution, which causes the excited carrier distribution to be asymmetric on the two sides of the conduction band. The longitudinal component of the optical current depends on τ^2 , whereas the Hall current contribution behaves like τ .

The trigonal warping or strain process is important to produce nonlinear optical phenomena based on the anisotropic Fermi surface. This approach can be utilized to extract the experimentally unknown trigonal wrapping by considering a system with linearly and circularly polarized light using scanning photocurrent microscopy. The difference of DC optical responses increases by the trigonal warping. Therefore, by measuring a significant difference in the value of the responses of the system at the optical band edge, the role of the trigonal warping should be recognized.

The impact of the Coulomb interaction on the DC current is a pertinent question. Since in an absorption photon a pair of the electron and hole are created therefore a new state emerges owing to Coulomb interaction [66]. This new state leads to additional absorption peaks shifted from the fundamental absorption edge by the coupling energies. Therefore, the DC nonlinear optical current should be enhanced when many-body effects are captured through the Bethe-Salpeter equation. Moreover, spin photocurrent is another subject that can be studied by including the spin-orbit interaction term in the system.

ACKNOWLEDGMENTS

We thank D. Culcer and M. Alidoosti for fruitful discussions. This work was supported by the Iran Science Elite (Grant No. M1400138).

APPENDIX: SHIFT CURRENT IN MONOLAYER MoS₂ WITH BROKEN SYMMETRIES

Monolayer MoS₂ has two valley minima at \mathbf{K} and \mathbf{K}' . The symmetry point group at the \mathbf{K} point is C_{3h} which contains the discrete symmetries C_3 (threefold rotation), C_3^2 , σ_h (reflection by the xy plane), S_3 (improper rotation $\sigma_h C_3$), and S_3^2 . The former prohibits nonlinear responses like the circular photovoltaic effect [51] and the fact that crystals with C_{3h} , D_{3h} , and T_d show only the linear photovoltaic effect if the total angular momentum allows the optical transition where $\Delta l = \pm 1$. There are several ways to activate the DC nonlinear optical response by imposing an in-plane electric field [67], vertical gate potential, and strain [68] to break the threefold symmetry. The doped MoS₂, through single-bias voltage breaking the mirror symmetry, reduces the point group and thus we consider a biased system.

Let us consider a low-energy $\mathbf{k} \cdot \mathbf{p}$ continuum model Hamiltonian around \mathbf{K} and \mathbf{K}' points system [61]:

$$\mathcal{H}_0 = \frac{\Delta + \lambda S \tau_v}{2} \sigma_z + t_0 a_0 \mathbf{k} \cdot \boldsymbol{\sigma} + \frac{\hbar^2 k^2}{4m_0} (\alpha + \beta \sigma_z), \quad (\text{A1})$$

and the trigonal warping \mathcal{H}_w contribution is given by

$$\mathcal{H}_w = t_1 a_0^2 (\mathbf{k} \cdot \boldsymbol{\sigma}_{\tau_v}^*) \sigma_x (\mathbf{k} \cdot \boldsymbol{\sigma}_{\tau_v}^*), \quad (\text{A2})$$

where the Pauli matrices $\boldsymbol{\sigma} = (\tau_v \sigma_x, \sigma_y)$ acts on the two-component wave functions. The spin-orbit couplings in the valence and conduction bands are considered and $\tau_v = \pm$ is a valley index, and $S = \pm$ refers to a spin index. Notice that $\mathbf{k} = k(\cos \theta, \sin \theta)$. All terms in the Hamiltonian are related to broken spatial inversion symmetry in monolayer TMD. In the case of monolayer MoS₂, all parameters are $a_0 = a/\sqrt{3}$, $a = 3.16 \text{ \AA}$, $\Delta = 1.82 \text{ eV}$, $\lambda_0 = 69 \text{ meV}$, $\lambda = -80 \text{ meV}$, $t_0 =$

2.34 eV , $t_1 = -0.14 \text{ eV}$, $\alpha = -0.01$, and $\beta = -1.54$. Notice that $\Delta l = -\tau_v$ in MoS₂ and thus circularly polarized light is considered.

The vertical bias breaks the mirror symmetry σ_h and thus modifies the on-site energies of atoms in three sublayers of TMDs. We assume a single-gate device in which the induced potentials take the values $U^b = 0$ and $U^t = 2U$ for layers. Using simple electronic arguments, the induced potentials for an applied vertical bias V can be estimated as $U = e \frac{d}{L} \frac{\epsilon'}{\epsilon} V$ where ϵ , d , ϵ' , and L denote the dielectric constants and thickness of ML-MDS and the substrate, respectively. Based on Ref. [61] we have $\delta \Delta = -0.1 + 0.2(U + 0.5)$, $\delta t_0 = 0.055 - 0.1(U + 0.55)$, $\delta \alpha = -0.15U/\text{eV}$, $\delta \beta = -1.95U/\text{eV}$.

The shift current was proposed, which attributes the charge separation arising from the asymmetry in the electron and hole wave functions [69]. This is an intrinsic effect of the shift current. A two-band model Hamiltonian was considered to explore the interband optical transition. The Floquet Hamiltonian is coupled by time-dependent terms $\langle u_c | \frac{1}{T} \int H[\mathbf{k} - \mathbf{A}(t)] e^{i\omega t} dt | u_v \rangle$. The nonlinear optical response $J_j = \sum_{i=x,y} \chi_j^{ii} E_i E_i$ is given by

$$\chi^{ii} = \frac{\pi e^3}{\hbar^2 \omega^2} \int \frac{d\mathbf{k}}{(2\pi)^d} \delta(\epsilon_{\mathbf{k}}^c - \epsilon_{\mathbf{k}}^v - \hbar\omega) |v_{vc}^i|^2 \times (\nabla_{\mathbf{k}} \phi_{cv}^i + \mathcal{R}^{cc} - \mathcal{R}^{vv}), \quad (\text{A3})$$

where i and j are Cartesian coordinates and $\phi_{cv}^i = \text{Im}(\log v_{cv}^i)$ maintains the gauge invariant. The interband velocity is also defined as $v_{cv} = i(\epsilon_{\mathbf{k}}^c - \epsilon_{\mathbf{k}}^v) \mathcal{R}^{vc}$. The Dirac δ function in our calculations is simulated by a Gaussian function with the broadening factor 0.01.

Figure 7 shows numerical results based on the shift current formalism for $U = -0.04 \text{ eV}$ in comparison with quantum kinetic theory. In MoS₂, the system is nonpolar and the conduction and valence bands are made effectively by d orbitals where charge carriers are less mobile. Therefore, the shift current tends to be remarkably small as shown in Fig. 7 and, subsequently, it is necessary to treat the nonlinear optical current as a kinetic phenomenon that is missing in the shift current [63].

-
- [1] M. G. Papadopoulos, A. J. Sadlej, J. Leszczynski *et al.*, *Non-Linear Optical Properties of Matter* (Springer, The Netherlands, 2006).
- [2] R. W. Boyd, *Nonlinear Optics* (Elsevier Science and Technology; Academic Press, London, 2020).
- [3] S. A. Mikhailov, *Europhys. Lett.* **79**, 27002 (2007).
- [4] D. Hsieh, Y. Xia, L. Wray, D. Qian, A. Pal1, J. H. Dil, J. Osterwalder, F. Meier, G. Bihlmayer, C. L. Kane, Y. S. Hor, R. J. Cava, and M. Z. Hasan, *Science* **323**, 919 (2009).
- [5] Y. L. Chen, J.-H. Chu, J. G. Analytis, Z. K. Liu, K. Igarashi, H. H. Kuo, X. L. Qi, S. K. Mo, R. G. Moore, D. H. Lu, M. Hashimoto, T. Sasagawa, S. C. Zhang, I. R. Fisher, Z. Hussain, and Z. X. Shen, *Science* **329**, 659 (2010).
- [6] M. Z. Hasan and C. L. Kane, *Rev. Mod. Phys.* **82**, 3045 (2010).
- [7] L. Fu, C. L. Kane, and E. J. Mele, *Phys. Rev. Lett.* **98**, 106803 (2007).
- [8] J. E. Moore and L. Balents, *Phys. Rev. B* **75**, 121306(R) (2007).
- [9] D. Xu, S. K. Yip, and J. A. Sauls, *Phys. Rev. B* **51**, 16233 (1995).
- [10] I. Žutić and O. T. Valls, *Phys. Rev. B* **58**, 8738 (1998).
- [11] Y. Tokura and N. Nagaosa, *Nat. Commun.* **9**, 3740 (2018).
- [12] Y. Gao and D. Xiao, *Phys. Rev. Lett.* **122**, 227402 (2019).
- [13] L. D. Tzuan, K. Fang, P. Nussenzveig, S. Fan, and M. Lipson, *Nat. Photonics* **8**, 701 (2014).
- [14] J. Kim, M. C. Kuzyk, K. Han, H. Wang, and G. Bahl, *Nat. Phys.* **11**, 275 (2015).
- [15] L. Shao, W. Mao, S. Maity, N. Sinclair, Y. Hu, L. Yang, and M. Lončar, *Nat. Electron.* **3**, 267 (2020).
- [16] G. Pacchioni, *Nat. Rev. Mater.* **4**, 514 (2019).
- [17] Q. Ma, S.-Y. Xu, H. Shen, D. MacNeill, V. Fatemi, T.-R. Chang, A. M. M. Valdivia, S. Wu, Z. Du, C.-H. Hsu *et al.*, *Nature (London)* **565**, 337 (2019).

- [18] Z. Du, C. Wang, S. Li, H.-Z. Lu, and X. Xie, *Nat. Commun.* **10**, 3047 (2019).
- [19] X.-L. Qi and S.-C. Zhang, *Phys. Today* **63**(1), 33 (2010).
- [20] C.-X. Liu, S.-C. Zhang, and X.-L. Qi, *Annu. Rev. Condens. Matter Phys.* **7**, 301 (2016).
- [21] S. Nandy and I. Sodemann, *Phys. Rev. B* **100**, 195117 (2019).
- [22] N. A. Sinitsyn, A. H. MacDonald, T. Jungwirth, V. K. Dugaev, and J. Sinova, *Phys. Rev. B* **75**, 045315 (2007).
- [23] I. Sodemann and L. Fu, *Phys. Rev. Lett.* **115**, 216806 (2015).
- [24] H. A. Hafez, S. Kovalev, J.-C. Deinert, Z. Mics, B. Green, N. Awari, M. Chen, S. Germanskiy, U. Lehnert, J. Teichert *et al.*, *Nature (London)* **561**, 507 (2018).
- [25] S.-Y. Hong, J. I. Dadap, N. Petrone, P.-C. Yeh, J. Hone, and R. M. Osgood, *Phys. Rev. X* **3**, 021014 (2013).
- [26] G. Soavi, G. Wang, H. Rostami, D. G. Purdie, D. De Fazio, T. Ma, B. Luo, J. Wang, A. K. Ott, D. Yoon *et al.*, *Nat. Nanotechnol.* **13**, 583 (2018).
- [27] I. Al-Naib, M. Poschmann, and M. M. Dignam, *Phys. Rev. B* **91**, 205407 (2015).
- [28] B. Endres, M. Ciorga, M. Schmid, M. Utz, D. Bougeard, D. Weiss, G. Bayreuther, and C. Back, *Nat. Commun.* **4**, 2068 (2013).
- [29] I. Žutić, J. Fabian, and S. Das Sarma, *Phys. Rev. Lett.* **88**, 066603 (2002).
- [30] H. Watanabe and Y. Yanase, *Phys. Rev. X* **11**, 011001 (2021).
- [31] V. Belinicher and B. I. Sturman, *Sov. Phys. Usp.* **23**, 199 (1980).
- [32] V. Belinicher, *Phys. Lett. A* **66**, 213 (1978).
- [33] E. L. Ivchenko, Y. B. Lyanda-Geller, G. E. Pikus, and R. Y. Rasulov, *Sov. Phys. Semicond.* **18**, 94 (1984).
- [34] J. B. Khurgin, *J. Opt. Soc. Am. B* **11**, 2492 (1994).
- [35] R. von Baltz and W. Kraut, *Phys. Rev. B* **23**, 5590 (1981).
- [36] V. Fridkin, *Crystallogr. Rep.* **46**, 654 (2001).
- [37] T. Rangel, B. M. Fregoso, B. S. Mendoza, T. Morimoto, J. E. Moore, and J. B. Neaton, *Phys. Rev. Lett.* **119**, 067402 (2017).
- [38] T. H. Maiman, *Nature (London)* **187**, 493 (1960).
- [39] P. A. Franken, A. E. Hill, C. W. Peters, and G. Weinreich, *Phys. Rev. Lett.* **7**, 118 (1961).
- [40] M. A. Green *et al.*, *Third Generation Photovoltaics* (Springer, Switzerland, 2006).
- [41] B. M. Fregoso, *Phys. Rev. B* **100**, 064301 (2019).
- [42] G. B. Osterhoudt, L. K. Diebel, M. J. Gray, X. Yang, J. Stanco, X. Huang, B. Shen, N. Ni, P. J. Moll, Y. Ran *et al.*, *Nat. Mater.* **18**, 471 (2019).
- [43] M. Nakamura, S. Horiuchi, F. Kagawa, N. Ogawa, T. Kurumaji, Y. Tokura, and M. Kawasaki, *Nat. Commun.* **8**, 281 (2017).
- [44] Y. Zhang, T. Ideue, M. Onga, F. Qin, R. Suzuki, A. Zak, R. Tenne, J. Smet, and Y. Iwasa, *Nature (London)* **570**, 349 (2019).
- [45] B. R. Carvalho, Y. Wang, K. Fujisawa, T. Zhang, E. Kahn, I. Bilgin, P. M. Ajayan, A. M. De Paula, M. A. Pimenta, S. Kar *et al.*, *Nano Lett.* **20**, 284 (2020).
- [46] J. E. Sipe and A. I. Shkrebtii, *Phys. Rev. B* **61**, 5337 (2000).
- [47] R. Asgari and D. Culcer, *arXiv:2108.10438*.
- [48] S. Yang, J. Seidel, S. Byrnes, P. Shafer, C.-H. Yang, M. Rossell, P. Yu, Y.-H. Chu, J. Scott, J. Ager *et al.*, *Nat. Nanotechnol.* **5**, 143 (2010).
- [49] L. Wang, L. Huang, W. C. Tan, X. Feng, L. Chen, X. Huang, and K.-W. Ang, *Small Methods* **2**, 1700294 (2018).
- [50] T. Oka and H. Aoki, *Phys. Rev. B* **79**, 081406(R) (2009).
- [51] B. I. Sturman, V. M. Fridkin, and J. Bradley, *The Photovoltaic and Photorefractive Effects in Noncentrosymmetric Materials* (Routledge, London, New York, 2021).
- [52] K. Choi, Y. T. Lee, and S. Im, *Nano Today* **11**, 626 (2016).
- [53] N. Miao, W. Li, L. Zhu, B. Xu, J. Zhou, S. R. Elliott, and Z. Sun, *Nanoscale Horiz.* **5**, 1566 (2020).
- [54] Z. Guan, C.-S. Lian, S. Hu, S. Ni, J. Li, and W. Duan, *J. Phys. Chem. C* **121**, 3654 (2017).
- [55] H. Yang, Y. Ma, Y. Liang, B. Huang, and Y. Dai, *ACS Appl. Mater. Interfaces* **11**, 37901 (2019).
- [56] N. Kumar, S. Najmaei, Q. Cui, F. Ceballos, P. M. Ajayan, J. Lou, and H. Zhao, *Phys. Rev. B* **87**, 161403(R) (2013).
- [57] L. M. Malard, T. V. Alencar, Ana Paula M. Barboza, K. F. Mak, and A. M. de Paula, *Phys. Rev. B* **87**, 201401(R) (2013).
- [58] D. Culcer, A. Sekine, and A. H. MacDonald, *Phys. Rev. B* **96**, 035106 (2017).
- [59] A. Sekine, D. Culcer, and A. H. MacDonald, *Phys. Rev. B* **96**, 235134 (2017).
- [60] P. Bhalla, A. H. MacDonald, and D. Culcer, *Phys. Rev. Lett.* **124**, 087402 (2020).
- [61] H. Rostami, A. G. Moghaddam, and R. Asgari, *Phys. Rev. B* **88**, 085440 (2013).
- [62] F. G. Ghamsari and R. Asgari, *Plasmonics* **15**, 1289 (2020).
- [63] B. I. Sturman, *Phys. Usp.* **63**, 407 (2020).
- [64] F. T. Vasko and O. E. Raichev, *Quantum Kinetic Theory and Application* (Springer, 2005).
- [65] W. Schäfer and M. Wegener, *Semiconductor Optics and Transport Phenomena* (Springer Science & Business Media, Verlag, Berlin, Heidelberg, 2013).
- [66] G. Xu, T. Zhou, B. Scharf, and I. Žutić, *Phys. Rev. Lett.* **125**, 157402 (2020).
- [67] S. Wang, M. S. Ukharty, and R. Saito, *Phys. Rev. Research* **2**, 033340 (2020).
- [68] H. Rostami, R. Roldán, E. Cappelluti, R. Asgari, and F. Guinea, *Phys. Rev. B* **92**, 195402 (2015).
- [69] T. Morimoto and N. Nagaosa, *Phys. Rev. B* **94**, 035117 (2016).